Supplementary Information

Fluoride-Assisted Crystallization Regulation Enables Efficient and Stable Wide-Bandgap Perovskite Photovoltaic

Chao Su,[a] Rui Wang,[a] Junlei Tao,[a] Jinliang Shen,[a] Di Wang,[b] Lixin Wang,[a,c] Guangsheng Fu,[a,c] Shaopeng Yang,[*a,c] Mingjian Yuan[b] and Tingwei He [*a,c]

a Hebei Key Laboratory of Optic-electronic Information and Materials, College of Physics Science and Technology, Hebei University, Baoding 071002, China;

b Department of Chemistry, Nankai University, Tianjin 300071, China;

c Province-Ministry Co-construction Collaborative Innovation Center of Hebei Photovoltaic Technology, Hebei University, Baoding 071002, China;

[*] Corresponding author

Email: spyang@hbu.edu.cn, htw2022@hbu.edu.cn

1. Supplementary Characterizations and Measurements.

Absorption spectra were measured on a Hitachi U-3900/3900H UV-vis spectrophotometer.

Surface morphological characterizations of the perovskite films were performed by Field emission scanning electron microscope (SEM) (Nova NanoSEM450).

Thermal admittance spectroscopy analysis could be obtained by capacitance-frequency curve using PARSTAT 4000 was used to measure the capacitance-frequency curve. The energy profile of trap density of states could be fitted from the equation: $N_t(E_\omega) = -\frac{V_{bi}\, dC\ \omega}{eWd\omega k_B T}$. Where V_{bi} is the built in voltage, ω is angular frequency, e is the elementary charge, W is the depletion width, C is the capacitance, k_B is the Boltzmann constant and T is the temperature.

The contact angle of perovskite film was measured by Micro Capture Pro and analyzed by Image J software.

2. Supplementary Figures

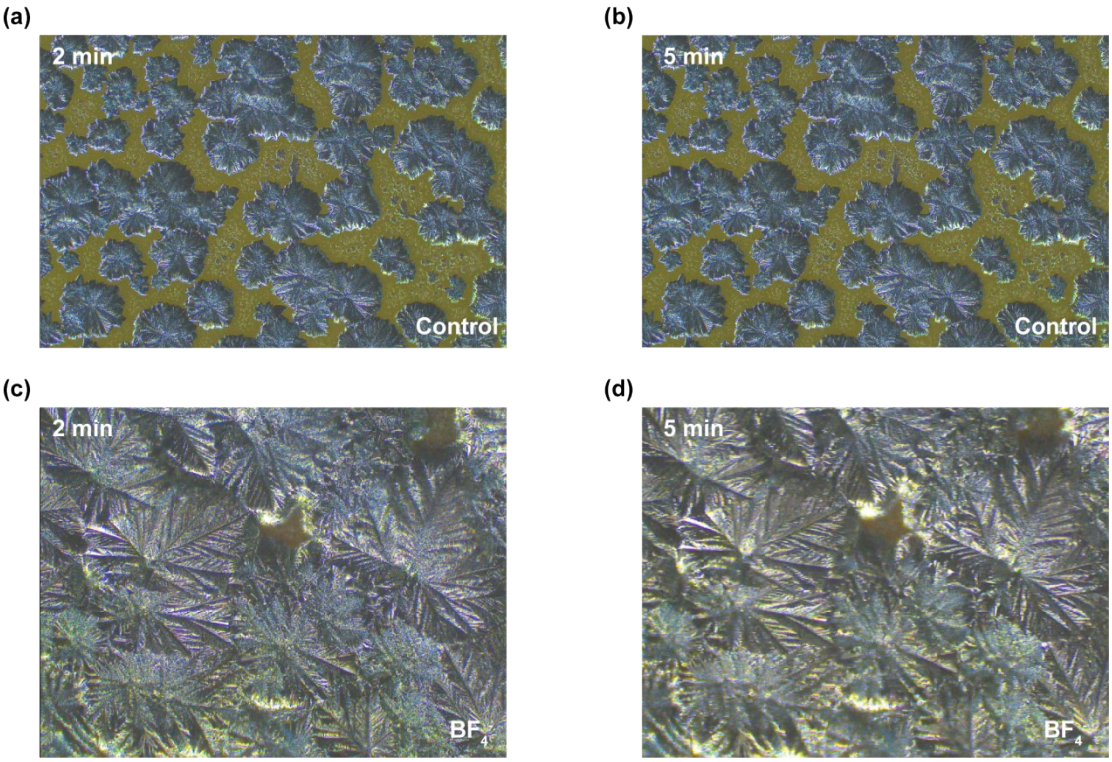

Fig. S1. The laser confocal microscope images of in-situ crystallization kinetics of perovskite precursor solution (a) at 2 min and (b) at 5 min. The laser confocal microscope images of in-situ crystallization kinetics of perovskite precursor solution with BF_4^- (c) at 2min and (d) at 5 min

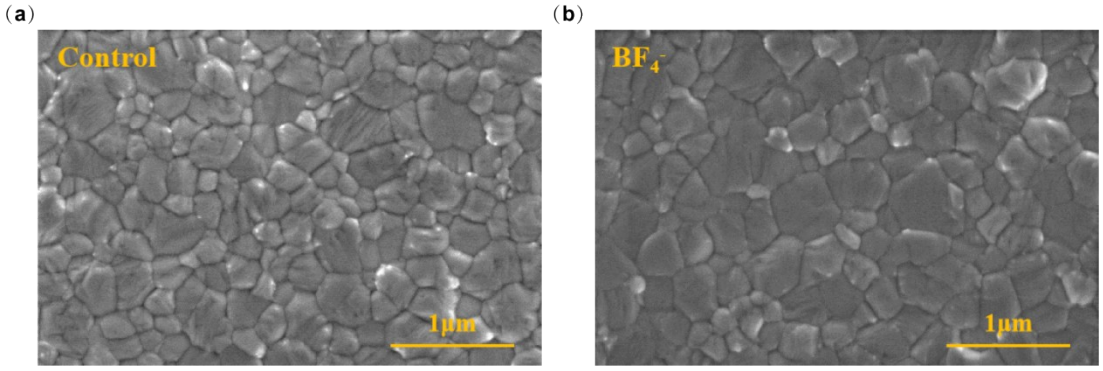

Fig. S2. (a) SEM imags of control perovskite films and (b) with BF_4^-.

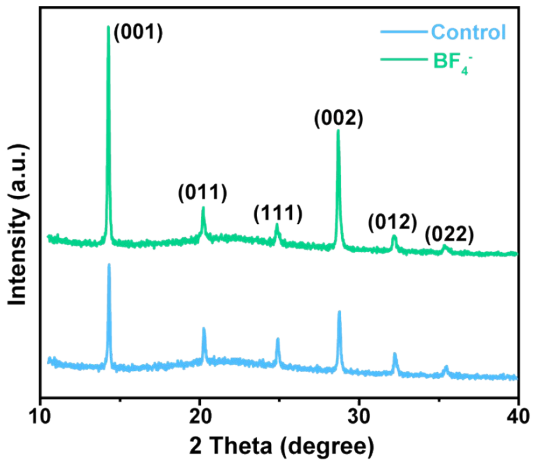

Fig. S3. XRD patterns of the perovskite films.

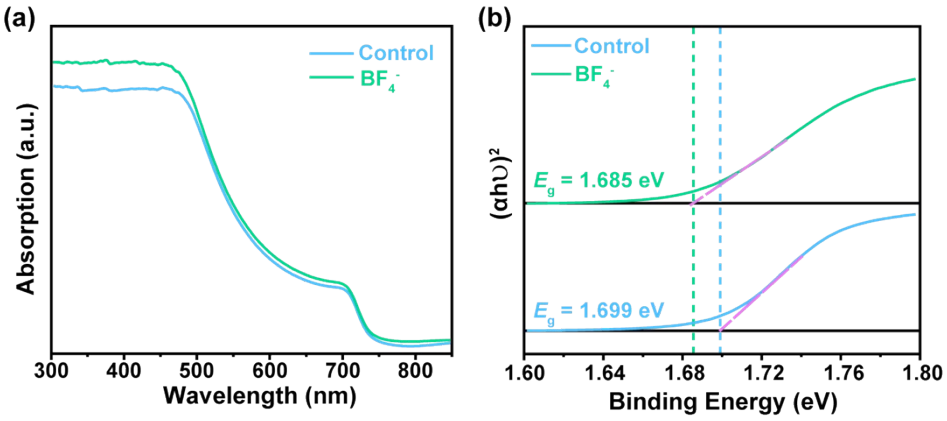

Fig. S4. (a) UV-vis absorbance spectra and (b) the relevant Tauc plot of the perovskite films.

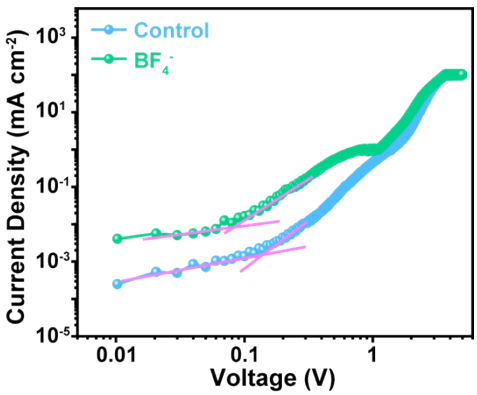

Fig. S5. Dark *J-V* Curves of ITO/PTAA/perovskite/Spiro-OMeTAD/Au structure.

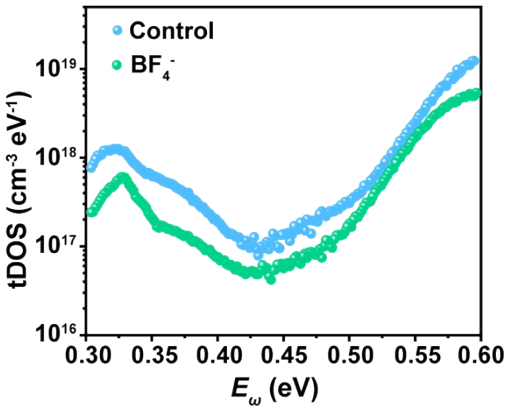

Fig. S6. Thermal admittance spectroscopy of wide-bandgap perovskite films.

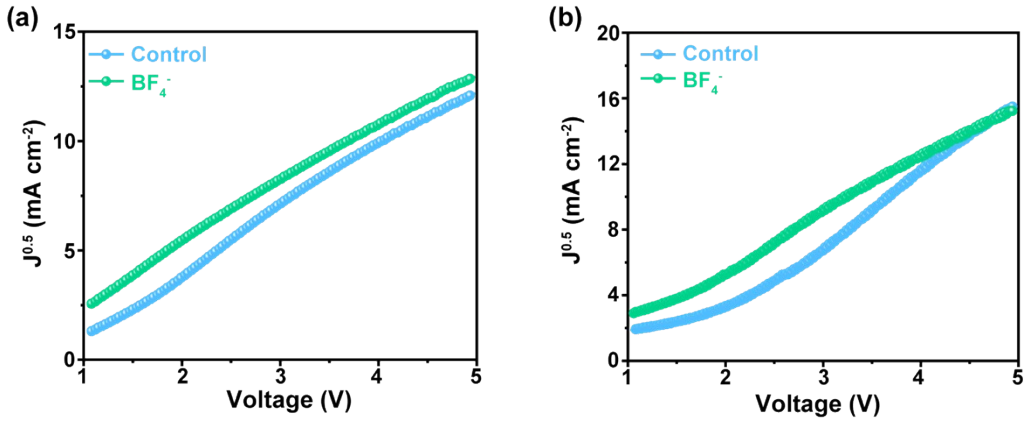

Fig. S7. (a) The electron mobility of the perovskite films using the SCLC model. (b) The hole mobility of the perovskite films using the SCLC model.

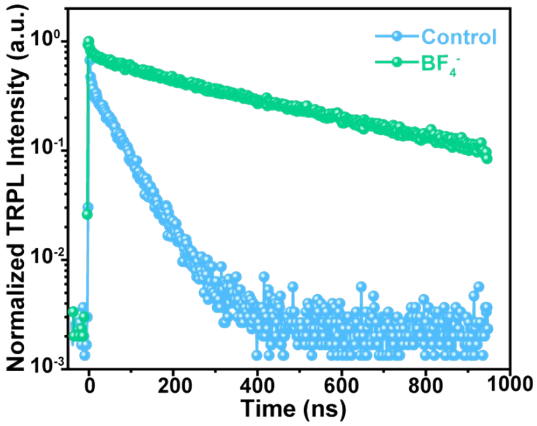

Fig. S8. TRPL spectra of the perovskite films.

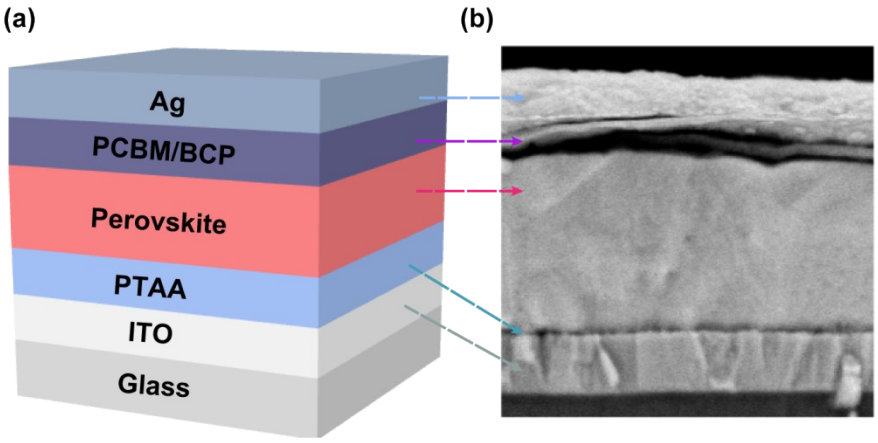

Fig. S9. (a) Schematic diagram of the device structure and (b) corresponding SEM sectional view.

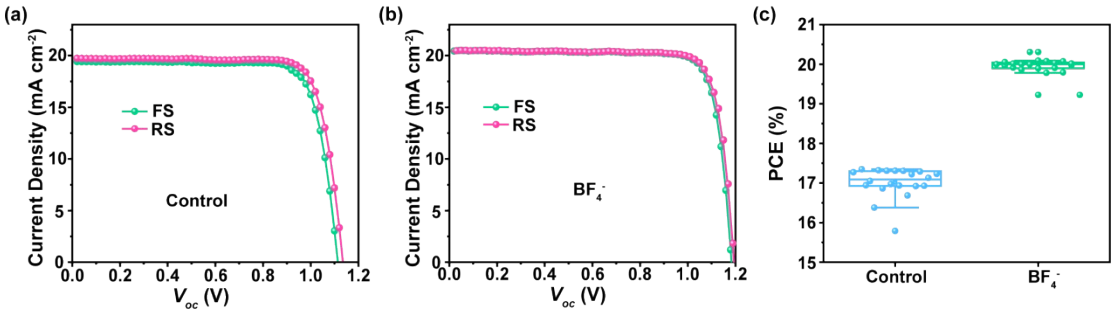

Fig. S10. The *J-V* curves of perovskite photovoltaics for different scanning directions of (a) without and (b) with BF_4^-. (c) PCE distribution of perovskite solar cells without and with BF_4^-.

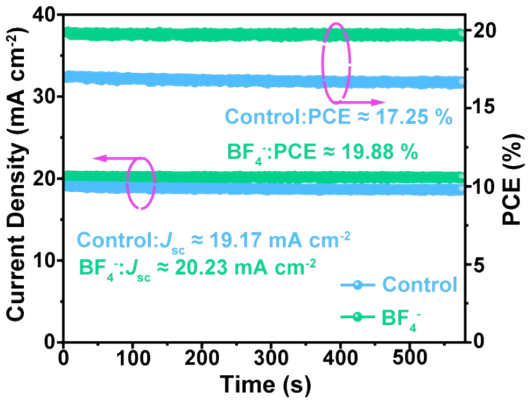

Fig. S11. Steady-state power output of PSCs at the maximum power point.

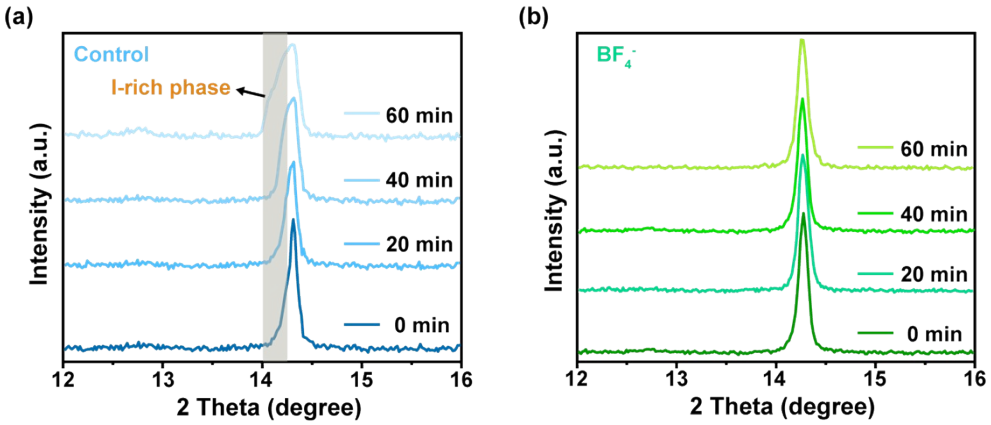

Fig. S12. XRD patterns of control and with BF_4^- at various times with 515 nm laser (100 mW cm^{-2}).

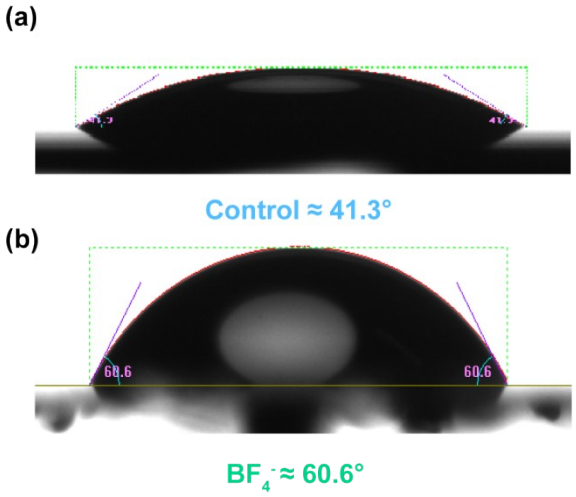

Fig. S13. (a) The water contact angles of control perovskite films and (b) with BF_4^-.

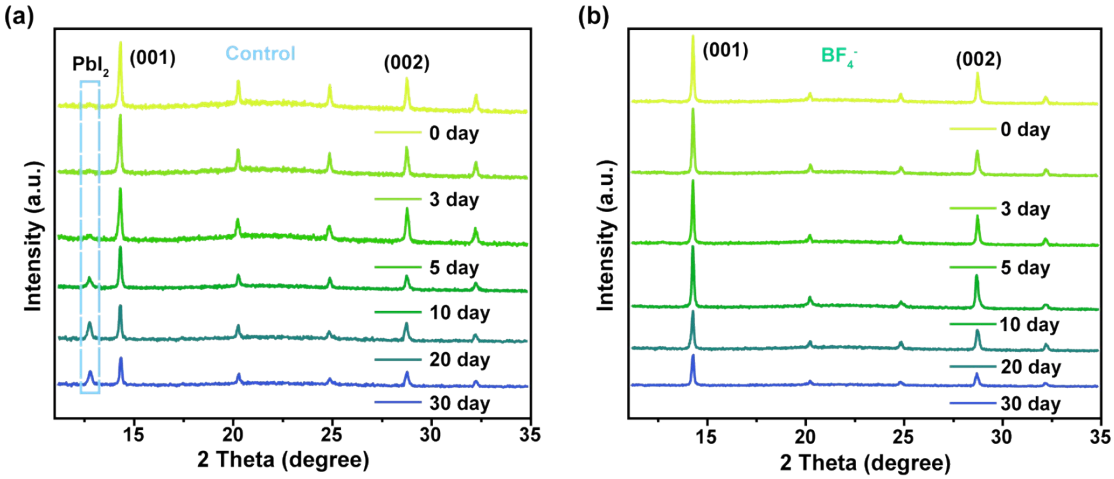

Fig. S14. XRD patterns of perovskite films deposited continuously for 30 days (a) control and (b) with BF_4^- ions under an atmospheric environment with 45-50% RH.

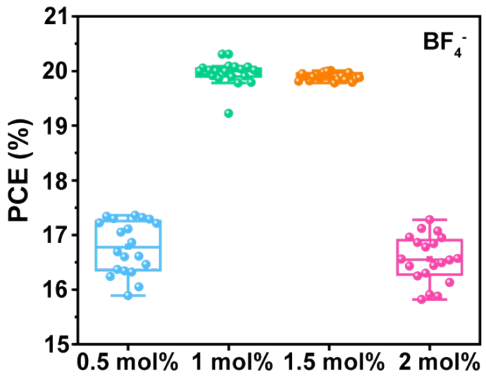

Fig. S15. The concentration optimization of BF_4^- in perovskite precursor solution.

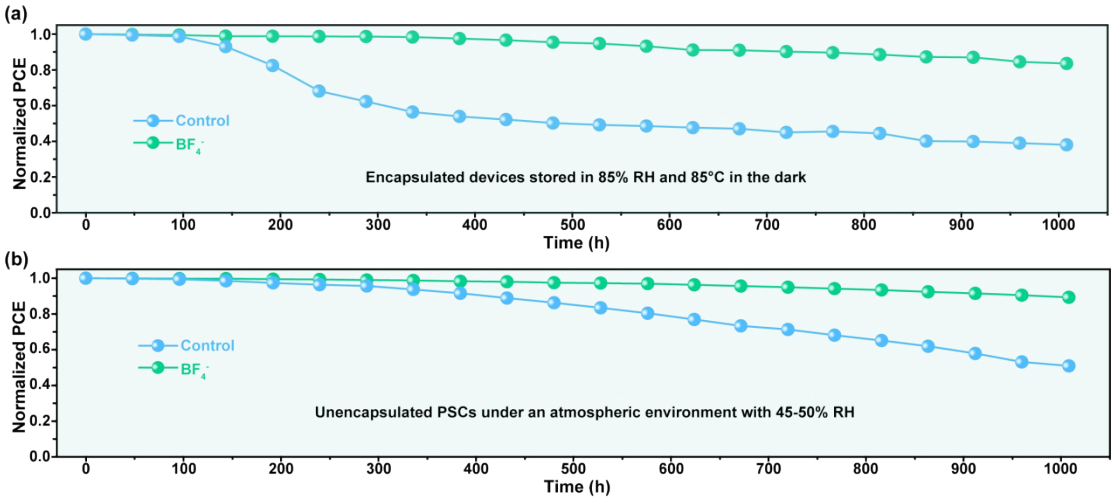

Fig. S16. (a) PCE evolution of encapsulated devices stored in 85% RH and 85℃ in the dark. (b) PCE evolution of unencapsulated PSCs under an atmospheric environment with 45-50% RH.

3. Supplementary Tables

Table S1. The FWHM values of (001) plan of perovskite films.

Sample	2Theta(θ) of 001	FWHM
Control	14.31	0.133
BF_4^-	14.27	0.127

Table S2. Parameters of μ_h, μ_e, μ_h/μ_e, and Trap Density (n_{trap}) of Perovskite Films.

Sample	μ_h ($cm^2 V^{-1} s^{-1}$)	μ_e ($cm^2 V^{-1} s^{-1}$)	μ_h/μ_e	n_{trap-e} (cm^{-3})	n_{trap-h} (cm^{-3})
Control	2.69×10^{-4}	1.79×10^{-4}	1.50	1.55×10^{16}	5.97×10^{15}
BF_4^-	1.74×10^{-4}	1.50×10^{-4}	1.16	4.44×10^{15}	3.48×10^{15}

Table S3. Photovoltaic parameters and hysteresis index of PSCs.

Devices	Direction	V_{oc} (V)	J_{sc} (mA cm^{-2})	FF	PCE (%)	*HI*
Control	FS	1.11	19.42	80.27	17.31	0.04
	RS	1.13	19.73	80.87	18.03	
BF_4^-	FS	1.18	20.43	83.33	20.09	0.01
	RS	1.19	20.46	83.34	20.29	

Table S4. The parameters of the TRPL spectra of perovskite films.

Sample	A_1 (%)	τ_1 (ns)	A_2 (%)	τ_2 (ns)	τ_{ave} (ns)
Control	59.39	2.36	40.61	63.82	60.67
BF_4^-	25.21	7.79	74.79	380.42	377.45

Table S5. EIS parameters for the PSCs.

Device	R_s (Ω)	C_{tr} (F)	R_{tr} (Ω)	C_{rec} (F)	R_{rec} (Ω)
Control	30.84	3.03×10^{-7}	958.82	9.27×10^{-9}	5558.09
BF_4^-	35.98	2.18×10^{-6}	928.31	7.53×10^{-9}	8560.11